# Supplemental Material for "Out-of-Time-Order Correlation as a Witness for Topological Phase Transitions"

Qian Bin,[1] Liang-Liang Wan,[1] Franco Nori,[2,3,4] Ying Wu,[1] and Xin-You Lü[1,*]

[1] *School of Physics and Institute for Quantum Science and Engineering, Huazhong University of Science and Technology, Wuhan, 430074, China*

[2] *Theoretical Quantum Physics Laboratory, RIKEN Cluster for Pioneering Research, Wako-shi, Saitama 351-0198, Japan*

[3] *RIKEN Center for Quantum Computing (RQC), 2-1 Hirosawa, Wako-shi, Saitama 351-0198, Japan*

[4] *Physics Department, The University of Michigan, Ann Arbor, Michigan 48109-1040, USA*

(Dated: January 24, 2023)

This supplemental material contains five parts: I. A detailed derivation of the analytical OTOC dynamics for the nearest-neighbor SSH model. II. Discussion of OTOC witness when the initial state is the eigenstate of the system. III. Additional discussion of the application of OTOC witness in the disordered systems. IV. Discussion of the application of OTOC witness in two-dimensional lattice described by the Qi-Wu-Zhang model. V. Discussion of the application of OTOC witness in the non-Hermitian systems.

## I. DERIVATION OF THE ANALYTICAL OTOC DYNAMICS

In this section, we present the analytical derivation of the OTOC dynamics in the system described by the 1D nearest-neighbor Su-Schrieffer-Heeger (SSH) model. We remind the Hamiltonian of the nearest-neighbor SSH model in the absence of disorder

$$H_{\rm s}=\sum_{n}\left\{\epsilon\nu a_{n}^{\dagger}\sigma_{1}a_{n}+\frac{\epsilon}{2}\left[a_{n+1}^{\dagger}(\sigma_{1}+i\sigma_{2})a_{n}+\text{h.c.}\right]\right\}, \tag{S1}$$

where $\sigma_j$ $(j=0,1,2,3)$ are the Pauli matrices, corresponding to the identity matrix $I$, $\sigma_x$, $\sigma_y$, and $\sigma_z$, respectively. Here $a_n^{\dagger}=(a_{n,A}^{\dagger},a_{n,B}^{\dagger})$ is the annihilation operator of the unit cell $n$ with sublattices $A$, $B$, and $\epsilon$ ($\epsilon\nu$) is the intercell (intracell) hopping strength. The parameter regimes $\nu<1$ and $\nu>1$ correspond to the topological non-trivial and trivial phases, respectively. This model has a chiral symmetry defined by a chiral operator $\mathcal{C}_{1\rm d}=\sum_n a_n^{\dagger}\sigma_3 a_n$ satisfying $[H_{\rm s},\mathcal{C}_{1\rm d}]_+=0$. By defining $V=V\rho_0=|\psi_0\rangle\langle\psi_0|$, the constructed OTOC becomes an experimentally feasible fidelity of the final state $\rho_f$ projected onto an initial state $\rho_0$, with

$$\mathcal{O}(t)=\text{tr}[\rho_0 e^{iH_{\rm s}t}W^{\dagger}e^{-iH_{\rm s}t}\rho_0 e^{iH_{\rm s}t}We^{-iH_{\rm s}t}]. \tag{S2}$$

In the following, we address in turn the analytical solutions of the OTOC dynamics for different choices of the operator $W$ and the initial state $|\psi_0\rangle$.

We consider a general initial state

$$|\psi_0\rangle=\frac{1}{\sqrt{M}}\sum_{m=1}^{M}(-1)^{m-1}|m,A\rangle, \tag{S3}$$

where $M=1$ corresponds to $|\psi_0\rangle=|1,A\rangle$. The matrix of the SSH Hamiltonian $H_{\rm s}$ including $2N$ sites in single-particle space has an implicit formula for the eigenpairs when $\nu\neq1$[1]. Then it is very difficult to analytically calculate the OTOC dynamics under this Hamiltonian. Comparing the cases of including $2N$ sites and $2N+1$ sites, the numerical energy spectrum of the latter is hardly changed except for one zero energy level is added, when the value of $N$ is large enough. The OTOC dynamics is almost not influenced by this extending of the Hamiltonian size. Thus, to analytically calculate the OTOC dynamics, we extend the size of the SSH model to $2N+1$ sites, and the Hamiltonian

* xinyoulu@hust.edu.cn

$H_{\rm s}$ becomes

$$H_{\rm s}=\epsilon\begin{pmatrix} 0 & \nu & & & & \\ \nu & 0 & 1 & & & \\ & 1 & 0 & \nu & & \\ & & \ddots & \ddots & \ddots & \\ & & & \nu & 0 & 1 \\ & & & & 1 & 0 \end{pmatrix}_{(2N+1)\times(2N+1)} . \tag{S4}$$

The eigenvalues of Eq. (S4) are

$$\lambda_0=0, \qquad \lambda_{\pm}^{(k)}=\pm\epsilon\sqrt{1+\nu^2+2\nu\cos\left(\frac{k\pi}{N+1}\right)}, \qquad (k=1,2,\dots N) \tag{S5}$$

and the corresponding eigenstates are

$$V^{(0)}=\frac{1}{\sqrt{A_0}}\left[(-\nu)^0,0,(-\nu)^1,0,(-\nu)^2,0,\dots,0,(-\nu)^{N-1},0,(-\nu)^N\right]^T \tag{S6}$$

and

$$\begin{aligned} V_{\pm}^{(k)}=&\frac{1}{\sqrt{A_{\pm}^{(k)}}}\left[\frac{1}{\nu}\sin\left(\frac{0k\pi}{N+1}\right)+\sin\left(\frac{k\pi}{N+1}\right),\frac{\lambda_{\pm}^{(k)}}{\epsilon\nu}\sin\left(\frac{k\pi}{N+1}\right),\frac{1}{\nu}\sin\left(\frac{k\pi}{N+1}\right)+\sin\left(\frac{2k\pi}{N+1}\right),\right.\\ &\frac{\lambda_{\pm}^{(k)}}{\epsilon\nu}\sin\left(\frac{2k\pi}{N+1}\right),\frac{1}{\nu}\sin\left(\frac{2k\pi}{N+1}\right)+\sin\left(\frac{3k\pi}{N+1}\right),\frac{\lambda_{\pm}^{(k)}}{\epsilon\nu}\sin\left(\frac{3k\pi}{N+1}\right),\dots,\\ &\left.\frac{1}{\nu}\sin\left(\frac{(N-1)k\pi}{N+1}\right)+\sin\left(\frac{Nk\pi}{N+1}\right),\frac{\lambda_{\pm}^{(k)}}{\epsilon\nu}\sin\left(\frac{Nk\pi}{N+1}\right),\frac{1}{\nu}\sin\left(\frac{Nk\pi}{N+1}\right)+\sin\left(\frac{(N+1)k\pi}{N+1}\right)\right]^T, \end{aligned} \tag{S7}$$

respectively, where

$$A_0=\sum_{n'=0}^{N}\nu^{2n'}=\begin{cases}(1-\nu^{2N+2})/(1-\nu^2) & (\nu\neq 1)\\ N+1 & (\nu=1)\end{cases}, \tag{S8}$$

$$A_{\pm}^{(k)}=\frac{(N+1)(\lambda_{\pm}^{(k)})^2}{\epsilon^2\nu^2}. \tag{S9}$$

In the space spanned by the eigenstates $\{V^{(0)},V_{\pm}^{(k)}\}$, the Hamiltonian $H_{\rm s}$ is given by

$$H_{\rm s}=\lambda^{(0)}|V^{(0)}\rangle\langle V^{(0)}|+\sum_{k=1}^{N}\left(\lambda_{+}^{(k)}|V_{+}^{(k)}\rangle\langle V_{+}^{(k)}|+\lambda_{-}^{(k)}|V_{-}^{(k)}\rangle\langle V_{-}^{(k)}|\right). \tag{S10}$$

Then we obtain the instantaneous state dominated by the forward evolution of $H_{\rm s}$, with

$$\begin{aligned} &e^{-iH_{\rm s}t}|\psi_0\rangle=\exp\{-i[\lambda^{(0)}|V^{(0)}\rangle\langle V^{(0)}|+\textstyle\sum_{k=1}^{N}(\lambda_{+}^{(k)}|V_{+}^{(k)}\rangle\langle V_{+}^{(k)}|+\lambda_{-}^{(k)}|V_{-}^{(k)}\rangle\langle V_{-}^{(k)}|)]t\}|\psi_0\rangle\\ &=\frac{1}{\sqrt{MA_0}}\sum_{m=1}^{M}\nu^{m-1}|V^{(0)}\rangle+\sum_{k=1}^{N}\sum_{m=1}^{M}\frac{(-1)^{m-1}}{\sqrt{M}}\left[\frac{1}{\nu}\sin(\frac{m-1}{N+1}k\pi)+\sin(\frac{mk\pi}{N+1})\right]\left[\frac{e^{-i\lambda_{+}^{(k)}t}}{\sqrt{A_{+}^{(k)}}}|V_{+}^{(k)}\rangle+\frac{e^{-i\lambda_{-}^{(k)}t}}{\sqrt{A_{-}^{(k)}}}|V_{-}^{(k)}\rangle\right]. \end{aligned} \tag{S11}$$

where

$$\langle V^{(0)}|m,A\rangle=\frac{1}{\sqrt{A_0}}(-\nu)^{m-1}, \quad \langle V_{\pm}^{(k)}|m,A\rangle=\frac{1}{\sqrt{A_{\pm}^{(k)}}}\left[\frac{1}{\nu}\sin\left(\frac{m-1}{N+1}k\pi\right)+\sin\left(\frac{mk\pi}{N+1}\right)\right], \tag{S12}$$

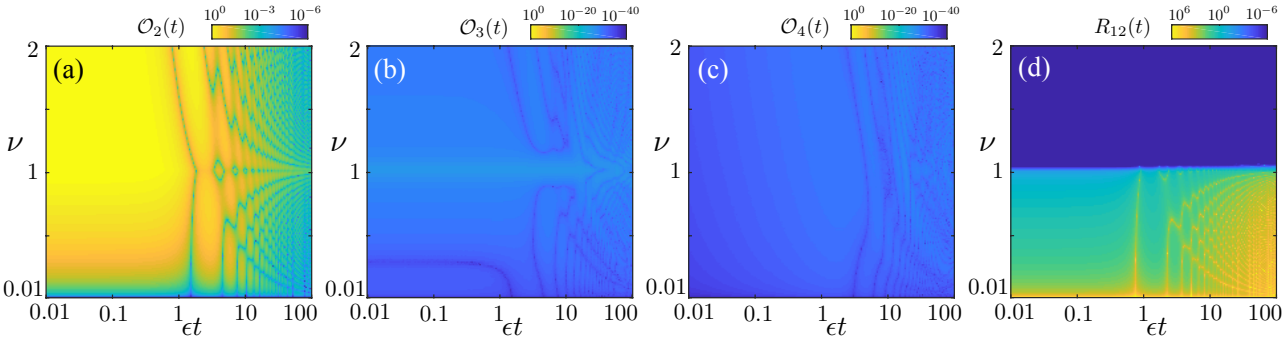


FIG. S1. The values of (a) $\mathcal{O}_2(t)$, (b) $\mathcal{O}_3(t)$, (c) $\mathcal{O}_4(t)$, and (d) $R_{12}(t)$ versus $\epsilon t$ and $\nu$ when $W = \sum_{n=1}^{N-1} a_n^\dagger \sigma_3 a_n$ and $|\psi_0\rangle = |1, A\rangle$. Other system parameters are $N = 200$ and $d_1 = d_2 = 0$.

and

$$\langle V^{(0)}|\psi_0\rangle = \frac{1}{\sqrt{MA_0}}(\nu^0 + \nu^1 + \nu^2 + \cdots + \nu^{M-1}) = \frac{1}{\sqrt{MA_0}} \sum_{m=1}^{M} \nu^{m-1}, \tag{S13}$$

$$\langle V_\pm^{(k)}|\psi_0\rangle = \frac{1}{\sqrt{MA_\pm^{(k)}}} \sum_{m=1}^{M} (-1)^{m-1} \left[\frac{1}{\nu} \sin\left(\frac{m-1}{N+1}k\pi\right) + \sin\left(\frac{mk\pi}{N+1}\right)\right]. \tag{S14}$$

When the OTOC operator $W = \sum_{l=1}^{L} a_l^\dagger(\sigma_3 + \sigma_0)a_l/2 = \sum_{l=1}^{L} a_{l,A}^\dagger a_{l,A}$ ($L = 1$ corresponds to the single-site operation), we obtain

$$\begin{aligned}
&\mathcal{O}(t) = \mathrm{tr}[\rho_0 e^{iH_s t} W^\dagger e^{-iH_s t} \rho_0 e^{iH_s t} W e^{-iH_s t}] \\
&= \left| \sum_{l=1}^{L} \left\{ \frac{(-\nu)^{l-1}}{A_0\sqrt{M}} \sum_{m=1}^{M} \nu^{m-1} + \sum_{k=1}^{N} \sum_{m=1}^{M} \frac{2(-1)^{m-1}\cos(\lambda_+^{(k)} t)}{\sqrt{M}A_+^{(k)}} \left[\frac{1}{\nu}\sin\left(\frac{m-1}{N+1}k\pi\right) + \sin\left(\frac{mk\pi}{N+1}\right)\right] \left[\frac{1}{\nu}\sin\left(\frac{l-1}{N+1}k\pi\right) + \sin\left(\frac{lk\pi}{N+1}\right)\right] \right\}^2 \right|^2 .
\end{aligned} \tag{S15}$$

This equation is reduced to Eq. (3) of the main text under the conditions of $L = 1$ and $M = 1$. When the OTOC operator $W = \sum_{n=1}^{N-1} a_n^\dagger \sigma_3 a_n = \sum_{n=1}^{N} a_n^\dagger \sigma_3 a_n - a_N^\dagger \sigma_3 a_N$, the OTOC function is reduced to

$$\mathcal{O}(t) = \mathrm{tr}[\rho_0 e^{iH_s t} W^\dagger e^{-iH_s t} \rho_0 e^{iH_s t} W e^{-iH_s t}] = |\mathcal{O}_1 + \mathcal{O}_2(t) - \mathcal{O}_3(t) + \mathcal{O}_4(t)|^2 \tag{S16}$$

where

$$\begin{aligned}
\mathcal{O}_1 &= \frac{1}{MA_0} \left( \sum_{m=1}^{M} \nu^{m-1} \right)^2 , \\
\mathcal{O}_2(t) &= \sum_{k=1}^{N} \frac{2\cos(2\lambda_+^{(k)} t)}{MA_\pm^{(k)}} \left[ \sum_{m=1}^{M} (-1)^{m-1} \left( \frac{1}{\nu}\sin(\frac{m-1}{N+1}k\pi) + \sin(\frac{mk\pi}{N+1}) \right) \right]^2 , \\
\mathcal{O}_3(t) &= \left| \frac{(-\nu)^{N-1}}{A_0\sqrt{M}} \sum_{m=1}^{M} \nu^{m-1} + \sum_{k=1}^{N} \sum_{m=1}^{M} \frac{2(-1)^{m-1}\cos(2\lambda_+^{(k)} t)}{\sqrt{M}A_\pm^{(k)}} [\frac{\sin(\frac{m-1}{N+1}k\pi)}{\nu} + \sin(\frac{mk\pi}{N+1})][\frac{\sin(\frac{N-1}{N+1}k\pi)}{\nu} + \sin(\frac{Nk\pi}{N+1})] \right|^2 , \\
\mathcal{O}_4(t) &= \left| \sum_{k=1}^{N} \sum_{m=1}^{M} \frac{-2i(-1)^{m-1}\lambda_+^{(k)} \sin(2\lambda_+^{(k)} t)}{\sqrt{M}A_\pm^{(k)}\epsilon\nu} [\frac{1}{\nu}\sin(\frac{m-1}{N+1}k\pi) + \sin(\frac{mk\pi}{N+1})] \sin(\frac{Nk\pi}{N+1}) \right|^2 .
\end{aligned} \tag{S17}$$

The terms $\mathcal{O}_2(t)$, $\mathcal{O}_3(t)$ and $\mathcal{O}_4(t)$ trend to zero over time, and $\mathcal{O}_3(t), \mathcal{O}_4(t) \ll \mathcal{O}_2(t)$ [see Figs. S1(a-c)]. Then the above OTOC function can be approximately reduced to $\mathcal{O}(t) \approx |\mathcal{O}_1 + \mathcal{O}_2(t)|^2$, and we can obtain the Eq. (4) of

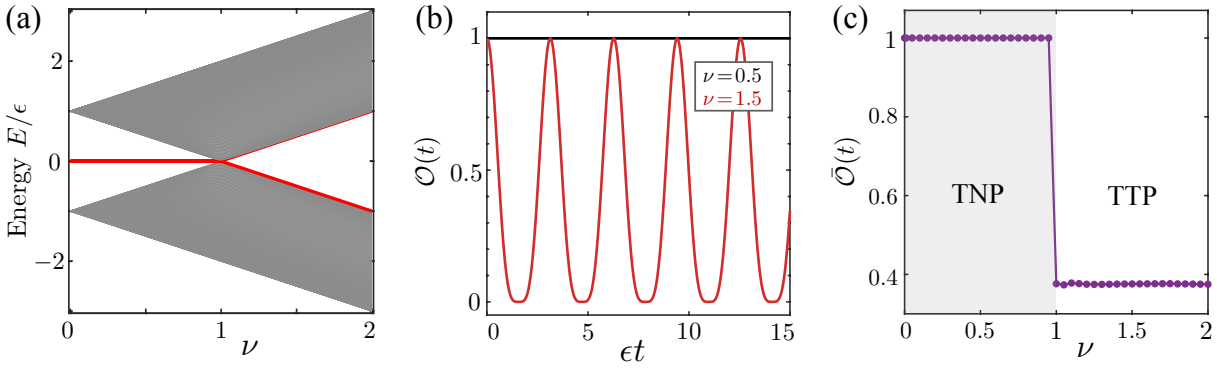


FIG. S2. (a) Energy spectrum of the 1D nearest-neighbor SSH model. (b) The evolution of the OTOC for different values of $\nu$, when the system is initially in the eigenstate $|\psi_E\rangle_{1d}$ of the system whose eigenvalue has the lowest absolute value, corresponding to the red curve of (a). (c) The average of the OTOC evolution $\bar{\mathcal{O}}(t)$ versus $\nu$. System parameters are $N = 200$ and $W = \sum_{n=1}^{N} a_{n,A}^{\dagger} a_{n,A}$. The gray and white areas correspond to the topological non-trivial phase (TNP) and topological trivial phase (TTP), respectively.

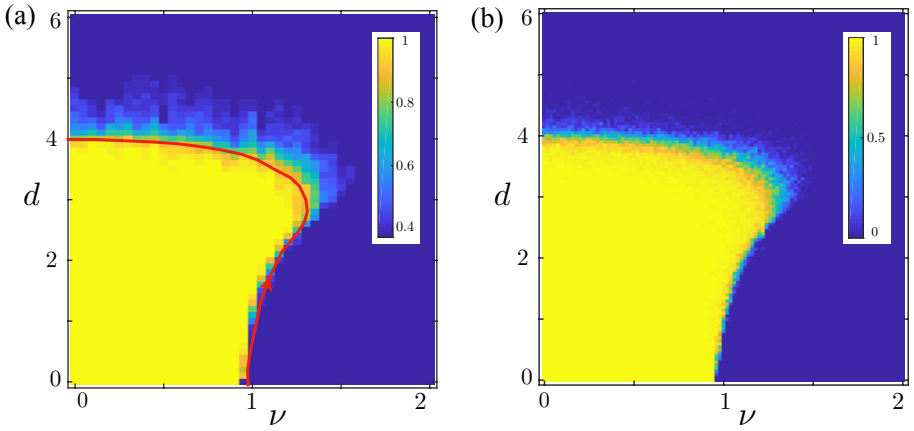


FIG. S3. Topological phase diagrams: (a) the averaged OTOC $\bar{\mathcal{O}}(t)$ versus disorder strength $d$ and $\nu$ when $W = \sum_{n=1}^{N} a_{n,A}^{\dagger} a_{n,A}$ and $|\tilde{\psi}_0\rangle = Q_{1d}|\psi_E\rangle_{1d}$; (b) the order parameter defined in Refs. [2, 3] versus disorder strength $d$ and $\nu$. Here all data are averaged over 30 independent disorder configurations, and $d_2 = 2d_1 = d$ and $N = 1000$.

the main text under the conditions of $L = 1$ and $M = 1$. We define the ratio $R_{12}(t) = \mathcal{O}_1/\mathcal{O}_2(t)$. As shown in Fig. S1(d), in the trivial phase $\nu > 1$, $R_{12}(t) \ll 1$ means that the analytical solution can be approximatively reduced to $\mathcal{O}(t) \approx \mathcal{O}_2^2(t)$, which evolves to almost zero in the long-time limit. In the non-trivial phase $\nu < 1$, we have $R_{12}(t \to \infty) \gg 1$ and the OTOC is reduced to $\mathcal{O}(t \to \infty) \approx \mathcal{O}_1^2$, which is a finite value. At the critical point $\nu = 1$, $R_{12}(t \to \infty) \approx 1$ corresponds to $\mathcal{O}(t \to \infty) \approx 0$. This can also be seen in the phase diagram Fig.1(e) of the main text. Note that $\nu \neq 0$ in the above equations, and $\nu = 0$ means that the hopping cannot occurs in the intercells. Here we have extended the size of the SSH model to $2N + 1$ sites, but these solutions Eqs. (S15-S17) are still valid for the system including $2N$ sites when the value of $N$ is large enough. In the main text, we have shown the numerical results obtained by numerically calculating Eq. (S2) for the system including $2N$ sites and the analytical results obtained by Eqs. (S15-S17) for the system including $2N + 1$ sites, respectively. The excellent agreement between the analytical solutions and fully numerical simulations demonstrates the validity of our approximation.

## II. THE OTOC WITNESS WHEN THE INITIAL STATE IS THE EIGENSTATE OF SYSTEM

In the section, we discuss the connection between OTOC dynamics and TPTs when the initial state is the eigenstate $|\psi_E\rangle_{1d}$ of the system whose eigenvalue has the lowest absolute value [see the red curve in Fig. S2(a)]. Let's take the system described by the the nearest-neighbor SSH model as an example. Applying an operation on the initial state, we obtain $|\tilde{\psi}_0\rangle = Q_s|\psi_E\rangle_{1d}$, where $Q_s = \sum_n a_n^{\dagger}(\sigma_0 + \sigma_3)a_n/2$. In the topological non-trivial phase $\nu < 1$, the

state $|\psi_E\rangle_{1d}$ is naturally an edge state of the system, e.g., the left edge state $\sum_n \alpha_n|n,A\rangle$ with $\sum_n |\alpha_n|^2 = 1$, and then $|\tilde{\psi}_0\rangle = Q_{1d}|\psi_E\rangle_{1d} = \sum_n \alpha_n|n,A\rangle = |\psi_E\rangle_{1d}$. The OTOC is reduced to $\mathcal{O}(t) = \mathrm{tr}[\tilde{\rho}_0^2] = 1$, which is a conserved quantity. The averaged OTOC function $\bar{\mathcal{O}}(t) = 1$. In the topological trivial phase $\nu > 1$, $|\psi_E\rangle_{1d}$ is not the edge state of the system, but a bulk state $|\psi_E\rangle_{1d} = \sum_n(\alpha_n|n,A\rangle + \beta_n|n,B\rangle)$, where $\sum_n(|\alpha_n|^2 + |\beta_n|^2) = 1$ and $\sum_n |\alpha_n|^2 = \sum_n |\beta_n|^2 = 1/2$. In Figs. S2(b,c), we show the OTOC dynamics and averaged OTOC in different topological phases when the OTOC operator $W = \sum_{n=1}^N a_{n,A}^\dagger a_{n,A} = \sum_{n=1}^N a_n^\dagger(\sigma_0 + \sigma_3)a_n/2$ and $|\tilde{\psi}_0\rangle = Q_s|\psi_E\rangle_{1d}$. The results are obtained by numerically calculating the OTOC function Eq. (S2), which demonstrates that the OTOC periodically oscillates in the topological trivial phase and becomes a conserved quantity in the topological non-trivial phase. The averaged OTOC $\bar{\mathcal{O}}(t)$ is thus discrete at the critical point, i.e., $\bar{\mathcal{O}}(t) = 0.375$ and $\bar{\mathcal{O}}(t) = 1$ in the trivial and non-trivial phases, respectively.

## III. ADDITIONAL DISCUSSION OF THE APPLICATION OF OTOC WITNESS IN THE DISORDERED SYSTEMS

We remind the Hamiltonian of the disordered nearest-neighbor SSH model

$$H_s = \sum_n \left\{ \nu_n a_n^\dagger \sigma_1 a_n + \frac{\omega_n}{2}\left[a_{n+1}^\dagger(\sigma_1 + i\sigma_2)a_n + \text{h.c.}\right]\right\}, \tag{S18}$$

where $\omega_n = \epsilon(1 + d_1 r_n)$ [or $\nu_n = \epsilon(\nu + d_2 r_n')$] is the intercell (or intracell) hopping strength. Disorder with the dimensionless strengths $d_1$, $d_2$ has been included here, and $r_n$, $r_n'$ are independent random real numbers chosen from the uniform distribution $[-0.5, 0.5]$. In the clean system (i.e., $d_1 = d_2 = 0$), the above equation is reduced to a standard SSH Hamiltonian Eq. (S1). Indeed, the symmetry-protected boundary state has strong robustness to weak disorder, but the topological features disappear as the disorder is too large. Moreover, the disorder can also induce the appearance of the non-trivial topology when it is added in a topological trivial structure. This disorder-driven topological phase is called as topological Anderson insulator phase. To fully show the effects of disorder on the TPTs, we numerically calculate the OTOC function Eq. (S2) with different system parameters by choosing the OTOC operator $W = \sum_{n=1}^N a_{n,A}^\dagger a_{n,A}$ and $|\tilde{\psi}_0\rangle = Q_{1d}|\psi_E\rangle_{1d}$. Figure S3(a) displays the dependence of the averaged OTOC $\bar{\mathcal{O}}(t)$ on the disorder strength $d$ and $\nu$, which can be considered as a topological phase diagram for the systems including disorders. There still exists an obvious step transition from 0.375 to 1 at the critical point in the presence of weak disorder. When the disorder is increased, the distinguishability of the OTOC dynamics disappear. Besides confirming the robustness of the OTOC witness to weak disorder, this phase diagram also shows topological Anderson insulator phase. For example, the system enters into the topological non-trivial phase from the trivial phase along with increasing the disorder strength, when the value of $\nu$ is slightly larger than 1. The physical mechanism for this result can be explained as follows. The relative strong disorder can induce an addition locality on the system, which leads a shift of the critical point of TPTs, as the red curve in Fig. S3(a). Then, in the phase diagram, there appears a range of $\nu$ corresponding to the occurrence of the TPT from the trivial to non-trivial phase with increasing disorder. Figure S3(b) shows the similar phase diagram from Refs. [2, 3]. Here, the topological phase diagram obtained by the OTOC witness is consistent with previous works, which verify the validity of our results.

## IV. THE APPLICATION OF OTOC WITNESS IN TWO-DIMENSIONAL LATTICE DESCRIBED BY THE QI-WU-ZHANG MODEL

In this section, we discuss the connection between OTOC dynamics and TPTs of 2D lattice system described by the Qi-Wu-Zhang model. As shown in Fig. S4(a), the Qi-Wu-Zhang model on the 2D square lattice has Hamiltonian [4, 5]

$$H_{qwz} = \sum_{x,y}\left\{\eta_0\left[a_{x+1,y}^\dagger\left(\frac{\sigma_3 + i\sigma_1}{2}\right)a_{x,y} + a_{x,y+1}^\dagger\left(\frac{\sigma_3 + i\sigma_2}{2}\right)a_{x,y} + \text{h.c.}\right] + \mu' a_{x,y}^\dagger\sigma_3\sigma_{x,y}\right\}, \tag{S19}$$

where $a_{x,y}^\dagger = (a_{x,y,A}^\dagger, a_{x,y,B}^\dagger)$ is the creation operator of the unit cell with sublattices $A$ and $B$, $\eta_0$ is the hopping strength, and $\mu'$ is the sublattice potential. The system does not have chiral symmetry. The topological trivial and non-trivial phases in the system can be identified by Chern number in momentum space. The parameter ranges $-2 < \mu'/\eta_0 < 2$ and $\mu'/\eta_0 = other$ correspond to topological trivial and non-trivial phases, respectively. In Fig. S4(b), we show that the OTOC of the system in the long-time limit $\mathcal{O}(t \to \infty)$ as a function of $\mu'/\eta_0$ when $W = \sum_{x,y} a_{x,y}^\dagger(\sigma_0 - \sigma_3)a_{x,y}/2$ and $|\psi_0\rangle = |1, A\rangle$, where $[W, H_{qwz}]_\pm \neq 0$. The distinct behavior of the OTOC dynamics in the trivial and

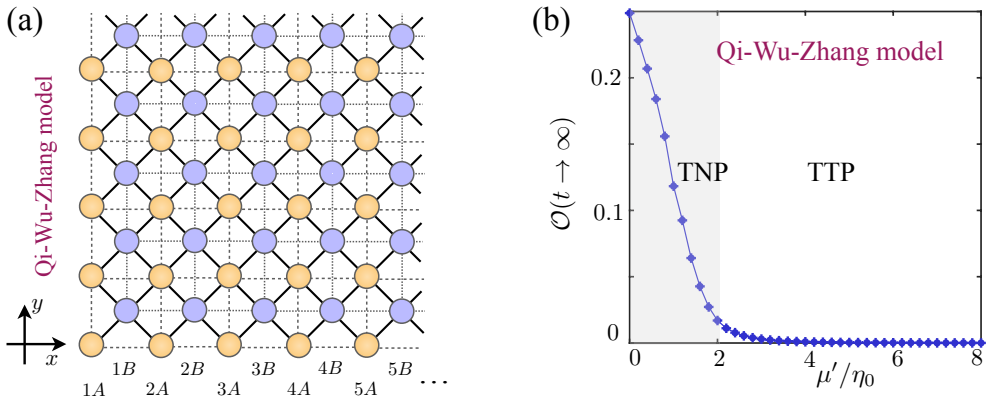


FIG. S4. (a) Scheme of the Qi-Wu-Zhang model. The unit cell consists of sublattices $A$ and $B$. (b) The OTOC in the long-time limit $\mathcal{O}(t\to\infty)$ versus $\mu'/\eta_0$. The TNP and TTP are indicated by the gray shading and write area, respectively. The cell numbers of $x$ and $y$ directions $N_x = N_y = 20$, and other system parameters are $W = \sum_{x,y} a^\dagger_{x,y}(\sigma_0 - \sigma_3)a^\dagger_{x,y}/2$ and $|\psi_0\rangle = |1, A\rangle$.

non-trivial phases is still observed in the system. The value of $\mathcal{O}(t\to\infty)$ changes from almost zero to the finite values, when the system enters into the non-trivial phase from the trivial phase.

## V. THE APPLICATION OF OTOC WITNESS IN NON-HERMITIAN SYSTEMS

In this section, we discuss the connection between TPTs and OTOC dynamics in non-Hermitian systems [6–10]. The Hamiltonian of the 1D non-Hermitian SSH model reads [11–14]

$$H_{\rm nh} = \sum_n \left\{ \frac{\epsilon(\nu+\delta)}{2} a_n^\dagger(\sigma_1 + i\sigma_2)a_n + \frac{\epsilon(\nu-\delta)}{2} a_n^\dagger(\sigma_1 - i\sigma_2)a_n + \frac{\epsilon}{2}\left[a_{n+1}^\dagger(\sigma_1 + i\sigma_2)a_n + \text{h.c.}\right]\right\}, \tag{S20}$$

where $\sigma_j$ $(j = 0, 1, 2, 3)$ are the Pauli matrices, corresponding to the identity matrix $I$, $\sigma_x$, $\sigma_y$, and $\sigma_z$, respectively. Here $a_n^\dagger = (a_{n,A}^\dagger, a_{n,B}^\dagger)$ is the annihilation operator of the unit cell $n$ with sublattices $A$, $B$, and $\epsilon$ is the intercell hopping strength, and $\epsilon(\nu+\delta)$ and $\epsilon(\nu-\delta)$ are the intracell hopping strength. When $\delta = 0$, Eq. (S20) is reduced to the standard SSH Hamiltonian (S1), with the phase transition point $\nu_c = 1$. When $\delta \neq 0$, Eq. (S20) is a non-Hermitian Hamiltonian, and the phase transition point is $\nu_c = \sqrt{1+\delta^2}$, where $\nu < \nu_c$ and $\nu > \nu_c$ correspond to the topological non-trivial and trivial phases, respectively.

Similar to the discussion in Hermitian systems, here we choose $|\psi_0\rangle = |1, A\rangle$, and take the OTOC operators $W = a_{1,A}^\dagger a_{1,A}$ and $W = \sum_{n=1}^{N-1} a_n^\dagger \sigma_3 a_n$ as examples, where $|n, A/B\rangle$ represents the system occupying in the sublattice $A/B$ of the unit cell $n$. As shown in Figs. S5(a,b), the OTOC becomes almost zero along with the time evolution in the trivial phase, while it trends to a non-zero finite value in the topological non-trivial phase. This means that the distinguished OTOC dynamics in the trivial and non-trivial phases can be obtained for two choices of the operator $W$. In Figs S5(c,d), we present the OTOC in the long-time limit $\mathcal{O}(t\to\infty)$ during a wide range of parameters, which shows a sudden change of the values of $\mathcal{O}(t\to\infty)$ at the phase transition point. The above results further demonstrate that the constructed OTOC can still be a witness for detecting TPTs even in non-Hermitian systems.


[1] B. C. Shin, A formula for eigenpairs of certain symmetric tridiagonal matrices, Bull. Austral. Math. Soc. **55**, 249 (1997).
[2] I. Mondragon-Shem, T. L. Hughes, J. T. Song, and E. Prodan, Topological Criticality in the Chiral-Symmetric AIII Class at Strong Disorder, Phys. Rev. Lett. **113**, 046802 (2014).
[3] E. J. Meier, F. A. An, A. Dauphin, M. Maffei, P. Massignan, T. L. Hughes, and B. Gadway, Observation of the topological Anderson insulator in disordered atomic wires, Science **362**, 929 (2018).
[4] X. -L. Qi, Y. -S. Wu, and S. -C. Zhang, Topological quantization of the spin Hall effect in two-dimensional paramagnetic semiconductors, Phys. Rev. B **74**, 085308 (2006).
[5] J. K. Asbóth, L. Oroszlány, and A. Pályi, *A Short Course on Topological Insulators* (Springer, 2016).

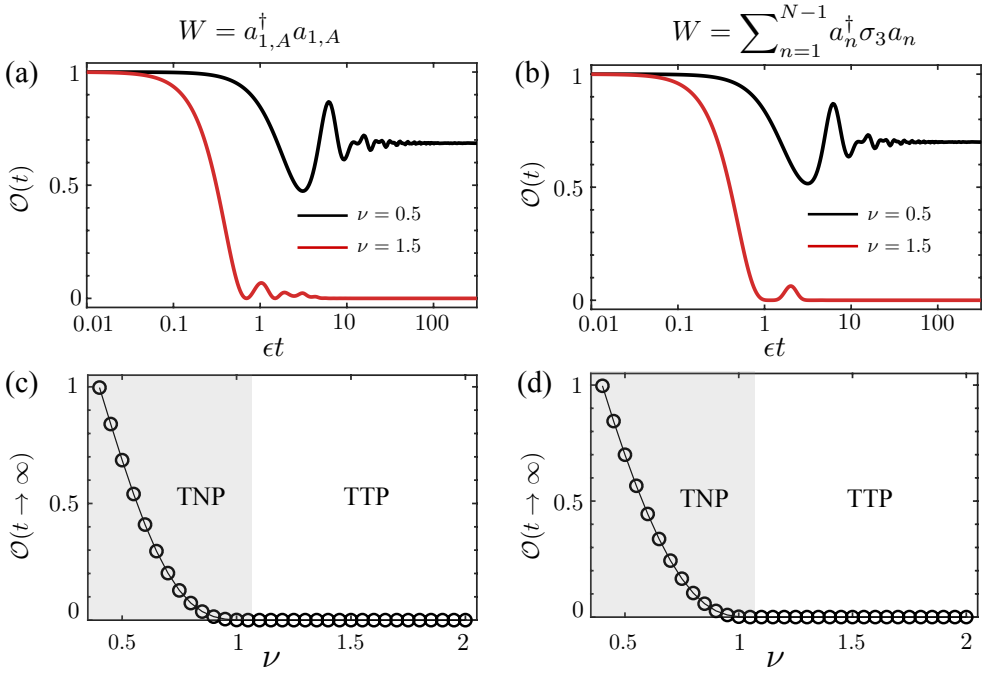


FIG. S5. (a–b) Dominated by $H_{\rm nh}$, the evolution of the OTOC for different values of $\nu$. (c–d) The OTOC in the long-time limit $\mathcal{O}(t \to \infty)$ versus $\nu$. The gray and white areas correspond to the TNP and TTP, respectively. Other system parameters are $\delta = 0.4$, $|\psi_0\rangle = |1, A\rangle$, (a,c) $W = a^\dagger_{1,A} a_{1,A}$, and (b,d) $W = \sum_{n=1}^{N-1} a^\dagger_n \sigma_3 a_n$.


[6] D. Leykam, K. Y. Bliokh, C. Huang, Y. D. Chong, and F. Nori, Edge Modes, Degeneracies, and Topological Numbers in Non-Hermitian Systems, Phys. Rev. Lett. **118**, 040401 (2017).
[7] C. Gneiting, A. Koottandavida, A.V. Rozhkov, and F. Nori, Unraveling the topology of dissipative quantum systems, Phys. Rev. Research **4**, 023036 (2022).
[8] F. Minganti, I. I. Arkhipov, A. Miranowicz, and F. Nori, Continuous Dissipative Phase Transitions with or without Symmetry Breaking, New J. Phys. **23**, 122001 (2021).
[9] C. Leefmans, A. Dutt, J. Williams, L. Q. Yuan, M. Parto, F. Nori, S. Fan, and A. Marandi, Topological dissipation in a time-multiplexed photonic resonator network, Nat. Phys. **18**, 442 (2022).
[10] L. Jin and Z. Song, Symmetry-Protected Scattering in Non-Hermitian Linear Systems, Chin. Phys. Lett. **38**, 024202 (2021).
[11] S. Lieu, Topological phases in the non-Hermitian Su-Schrieffer-Heeger model, Phys. Rev. B **97**, 045106 (2018).
[12] F. K. Kunst, E. Edvardsson, J. C. Budich, and E. J. Bergholtz, Biorthogonal Bulk-Boundary Correspondence in Non-Hermitian Systems, Phys. Rev. Lett. **121**, 026808 (2018).
[13] S. Y. Yao and Z. Wang, Edge States and Topological Invariants of Non-Hermitian Systems, Phys. Rev. Lett. **121**, 086803 (2018).
[14] C. H. Yin, H. Jiang, L. H. Li, R. Lü, and S. Chen, Geometrical meaning of winding number and its characterization of topological phases in one-dimensional chiral non-Hermitian systems, Phys. Rev. A **97**, 052115 (2018).